Published in final edited form as:

Science. 2018 August 03; 361(6401): 506–511. doi:10.1126/science.aar4056.

Cryo-EM structure of a mitochondrial calcium uniporter

Jiho Yoo[#1], **Mengyu Wu**[#2], **Ying Yin**[1], **Mark A. Herzik Jr**[2], **Gabriel C. Lander**[2,*], and **Seok-Yong Lee**[1,*]

[1]Department of Biochemistry, Duke University School of Medicine, Durham, North Carolina, 27710, USA.

[2]Department of Integrative Structural and Computational Biology, The Scripps Research Institute, La Jolla, California, 92037, USA.

[#] These authors contributed equally to this work.

One Sentence Summary:

The structure of MCU reveals a tetrameric architecture and provides the molecular framework for understanding the mechanism of calcium selectivity.

Abstract

Calcium transport plays an important role in regulating mitochondrial physiology and pathophysiology. The mitochondrial calcium uniporter (MCU) is a calcium-selective ion channel that is the primary mediator for calcium uptake into the mitochondrial matrix. Here we present the cryo-electron microscopy structure of the full-length MCU from *Neurospora crassa* to an overall resolution of ~3.7 Å. Our structure reveals a tetrameric architecture, with the soluble and transmembrane domains adopting different symmetric arrangements within the channel. The conserved W-D-Φ-Φ-E-P-V-T-Y sequence motif of MCU pore forms a selectivity filter comprising two acidic rings separated by one helical turn along the central axis of the channel pore. The structure combined with mutagenesis gives insight into the basis of calcium recognition.

Mitochondrial Ca^{2+} transport is critical for shaping the dynamics of intracellular calcium signaling, regulating energy metabolism, generating reactive oxygen species, and modulating cell death (1, 2). Ca^{2+} uptake across the mitochondrial inner membrane was shown to occur via a “uniporter” (3) and electrophysiological studies of the mitoplast inwardly-rectifying Ca^{2+} current (I_{MICA}) showed that this “uniporter” is an ion channel that exhibits a remarkable selectivity for Ca^{2+} (4). Recent genomics studies have identified the key components of the uniporter holocomplex (uniplex) (5–9). In vertebrates, it comprises

[*]Correspondence to: S.-Y. Lee, seok-yong.lee@duke.edu, telephone: 919-684-1005, G.C. Lander, glander@scripps.edu, telephone: 858-784-8793.

Author contributions: J.Y. conducted all biochemistry of MCU and the mitochondrial Ca^{2+} uptake assay under the guidance of S.-Y.L. M.H. performed negative-staining EM experiments, and M.W. conducted all cryo-EM experiments under the guidance of G.C.L and M.H. J.Y., Y.Y., M.H., and M.W. performed model building and refinement. All authors wrote the paper.

Competing interests: The authors declare no competing interests.

Data and materials availability: The coordinates are deposited in the Protein Data Bank with the PDB ID 6DT0 and the electron density maps have been deposited in EMDB with the ID EMD-8911. All data are available in the manuscript or the supplementary material.

the mitochondrial calcium uniporter (MCU), an auxiliary transmembrane protein essential MCU regulator (EMRE) (8), and the auxiliary EF hand-containing proteins mitochondrial calcium uptake 1 (MICU1) and MICU2 (6, 10). EMRE plays a dual role in maintaining MCU in an open state and recruiting MICU1/2 (11) that regulate the activity of MCU in a Ca^{2+}-dependent manner (6, 12–15). While MCU is widely distributed across all major branches of eukaryotes (16), EMRE is metazoan-specific (8). The MCU orthologue from *Dictyostelium discoideum*, an organism lacking EMRE, alone, is capable of reconstituting channel activity in yeast (17). In fungi, MCU is typically present without the MICU1/2 homologs (16). Recent studies have further shown that fungal MCU homologs are also able to reconstitute channel activity *in vitro* and *in vivo* on their own (18, 19). Taken together, these data establish that MCU is the Ca^{2+}-conducting pore-forming unit of the uniplex.

A single protomer of MCU is predicted to possess two transmembrane helices (TM1 and TM2), two coiled-coils (CC1 and CC2), and a N-terminal domain (NTD) located on the matrix side. All MCU homologs contain a highly-conserved sequence motif W-D-Φ-Φ-E-P-V-T-Y (Φ denotes hydrophobic amino acids) located between TM1 and TM2. This motif is oriented facing the intermembrane space and is thought to form the selectivity filter in the oligomeric channel (5, 7, 9). The NTD is composed of ~100 residues and extends into the mitochondrial matrix. Crystallographic studies of the human MCU NTD revealed a distinct structural fold similar to a beta-grasp, and subsequent functional studies revealed its modulatory role in MCU function (20, 21). A structure of the NTD-deleted MCU homolog from *C. elegans* (cMCU-ΔNTD) was recently determined using NMR and negative-stain electron microscopy, revealing a pentameric architecture (22), although the absence of the NTD limited further structural insights into the full-length channel assembly. We therefore conducted structural studies of a full-length MCU homolog using cryo-electron microscopy (cryo-EM). After screening a number of MCU homologues based on phylogenetic analyses (16), we found that a homolog from *Neurospora crassa* (MCU_{NC}) was suitable for structural studies. To prevent proteolysis, we introduced a Tyr232Ala mutation into a flexible loop within the NTD (fig. S1). This Tyr232Ala mutant eluted at a similar volume as wild-type MCU_{NC} during size-exclusion chromatography, and exhibited a similar overall architecture, as determined by negative-stain EM (fig. S2). MCU_{NC} was prepared under two different Ca^{2+} conditions for EM studies, referred to as low and high Ca^{2+} (see Methods). In both conditions, MCU_{NC} was reconstituted in amphipol and subjected to single-particle 3D cryo-EM analysis. Interestingly, MCU_{NC} unambiguously showed a tetrameric arrangement by EM under both Ca^{2+} conditions (fig. S3). The attainable resolution of these reconstructions (4.7–7 Å, fig. S3, see Methods) appeared to be limited by flexibility of the NTD. Therefore, we attempted to cross-link the NTD of MCU_{NC} using the water-soluble cross-linker bis-sulfosuccinimidyl suberate (BS3), in the presence of high Ca^{2+}, and reconstituted the BS3-crosslinked MCU_{NC} into nanodiscs for EM analyses. The 3D reconstruction of cross-linked MCU_{NC} in nanodiscs was determined to an overall resolution of ~3.7 Å (fig. S4). Comparison of the 3D reconstructions of cross-linked MCU_{NC} and native MCU_{NC} showed that cross-linking did not appreciably affect the structure of MCU_{NC} significantly (fig. S4). Thus, data of cross-linked and native MCU_{NC} were combined to yield an improved reconstruction at an overall resolution of ~3.7 Å (see Methods, fig. S4) that allowed for *de novo* model building (Methods and Table S1).

SDS-PAGE analysis of BS3-crosslinked MCU_{NC} indicated a complete conversion of the monomeric MCU band to a single band with an apparent molecular weight most compatible with tetrameric MCU_{NC} (fig. S2). Both cross-linked and native MCU_{NC} in detergent micelles elute at similar volumes during size-exclusion chromatography suggesting that cross-linking did not alter the oligomeric state of MCU_{NC}. Finally, 2D classification and asymmetric 3D classification of both the native and cross-linked MCU_{NC} samples unambiguously showed a tetrameric organization of MCU_{NC}, with no evidence for a pentamer, strongly supporting the tetrameric architecture of MCU_{NC} in our final structures (figs. S3 and S4).

The overall shape of the MCU_{NC} homotetramer is a prolate spheroid with dimensions of approximately 40 Å x 48 Å x 130 Å (Fig. 1). The transmembrane domain (TMD) is formed by TM1 and TM2 helices and the matrix region comprises the coiled-coil domain (CCD) and the NTD. TM1 and CC1 form a long and continuous helix at the periphery of the channel, while the TM2 helices line the central symmetry axis (Fig. 1B). The TM helices are arranged such that TM1 from one protomer primarily interacts with TM2 from the adjacent protomer (Fig. 1E). TM2 is followed by ~15 amino acids near the matrix-membrane interface but could not be accurately modeled (fig. S6). Immediately C-terminal to this region, a short helix, which we termed the junctional helix (JH), is positioned nearly perpendicular to TM1 and TM2 and forms a junction between TM2 and CC2. In the CCD, CC1 and CC2 form a dimeric coiled-coil, resulting in four dimeric coiled-coils within the tetramer. Due to the uncertainty of the connection between TM2 and JH, we cannot rule out the possibility that CC2 interacts with CC1 from the neighboring protomer (fig. S6). Unlike human MCU (hMCU), CC2 of MCU_{NC} is followed by three putative helical regions at its C-terminus, which is not resolved in the 3D reconstruction (fig. S1). The NTD comprises six β-strands (β1−β6) and two α-helices (α1-α2) and is connected to CC1 of the CCD. α2, located between the CCD and the rest of the NTD, positions the NTD relative to the rest of the channel (Fig. 1, C to E). Despite the low sequence identity (~17% for the structured regions), the NTD is structurally very similar to the hMCU NTD fragment (PDB ID: 5KUJ, Cα RMSD. 1.8 Å, figs. S1 and S7) (20, 21).

All MCU homologs contain the highly-conserved sequence motif W-D-Φ-Φ-E-P-V-T-Y, which has been proposed to form the selectivity filter (5, 7, 22). In our MCU_{NC} structure, this sequence motif is located in the N-terminal region of TM2 (Fig. 2) with the carboxylate side chains of conserved acidic residues Asp^{355} and Glu^{358} from each protomer directed towards the central symmetry axis, forming two acidic rings along the channel pore. The first acidic ring formed by Asp^{355}, which we term Site 1 (S1), is located at the mouth of the pore and exposed to the intermembrane space. The distances between diagonally positioned Asp^{355} are approximately 8.8 Å, indicating that a hydrated Ca^{2+} is likely to bind to this ring (Fig. 2C, S1). The second acidic ring formed by Glu^{358} is termed Site 2 (S2). Notably, there is an extensive network of interactions surrounding Glu^{358} involving residues in the W-D-Φ-Φ-E-P-V-T-Y motif that position the carboxylate group of Glu^{358} toward the central symmetry axis. Specifically, Pro^{359} appears to make inter-protomer CH-π interactions with Trp^{354} from the adjacent subunit, the amide nitrogen in the indole ring of Trp^{354} hydrogen bonds to the carboxylate group of Glu^{358} from an adjacent protomer, and Tyr^{362} is involved in both π-π interactions with Trp^{354} as well as hydrogen bonding interactions with Thr^{361}

from the adjacent protomer (Fig. 2, C and D, and fig. S4). Although the EM density for the MCU motif is sufficiently high to place side-chain atoms, the exact chemical nature of these interactions should be interpreted with caution. The distance between the carboxylate groups of Glu^{358} from diagonally opposing protomers is approximately 4.8 Å, suggesting that only dehydrated Ca^{2+} can be coordinated at S2. There is a strong EM density at the center of S2 (>17 σ, fig. S8A) that we tentatively assign to Ca^{2+} because: 1) the density peak is present in both an asymmetric reconstruction of MCU_{NC} as well as the corresponding half maps (fig. S8, B and C), and 2) calcium was present in high concentration during both protein purification and EM grid preparation (see Methods). The coordination of dehydrated Ca^{2+} by acidic residues has been observed in both TRPV6 and Orai1, and was proposed to be key to the Ca^{2+} selectivity of these channels (23, 24). We therefore suggest that, together, this S2 acidic ring plays an important role in the selective Ca^{2+} transport by MCU. Consistent with our structural observations, mutation of Glu^{358} has been shown to abolish hMCU activity (22). We also observed two polar amino acids, Thr^{361} and Tyr^{362}, located one helical turn below S2 that line the central axis of the pore, which we tentatively term “Site 3” (S3). The diagonal distances between the side chains are large (13–14 Å), so S3 may play a role in hydrating Ca^{2+} ions exiting S2. We observed an EM density at the center of S3, the identity of which is unclear (figs. S8, A to C). The selectivity filter organization of MCU_{NC} is in contrast with other classical tetrameric cation channels, where the selectivity filter is formed by loops connecting a TM helix and a pore helix (25, 26).

In order to investigate the role of the above-described interactions of the W-D-Φ-Φ-E-P-V-T-Y motif in Ca^{2+}-permeation by MCU, we employed site-directed mutagenesis and Ca^{2+}-uptake assays. Although functional assays are not currently available for MCU_{NC}, we exploited the high conservation of the selectivity filter within the MCU family and used an established mitochondrial Ca^{2+}-uptake assay in HEK-293 cells lacking hMCU to test the activity of transfected hMCU mutants designed based on our MCU_{NC} structure (11). Specifically, we tested the importance of Trp^{260}, Thr^{267}, and Tyr^{268} (Trp^{354}, Thr^{361}, and Tyr^{362} in MCU_{NC}) for Ca^{2+} uptake by hMCU (Fig. 2, E and F). Importantly, mutation of Trp^{260} (Trp^{354} in MCU_{NC}) to either phenylalanine or alanine abolished hMCU-mediated Ca^{2+} uptake and mutation of Thr^{267} (Thr^{361} in MCU_{NC}) or Tyr^{268} (Tyr^{362} in MCU_{NC}) to alanine reduced the hMCU-mediated Ca^{2+} uptake substantially, indicating their importance for MCU function. Notably, Ca^{2+} uptake was restored in the Tyr^{268} (Tyr^{362} in MCU_{NC}) to phenylalanine mutant, indicating that aromaticity is important for this position, in agreement with the above-described interactions. None of the tested mutations appreciably affected the expression level of hMCU compared to WT (Fig. 2F).

Viewing along the symmetry axis of the channel a symmetry mismatch occurs wherein the TMD adopts 4-fold symmetry while the CCD and the NTD show a 2-fold symmetric organization (Fig. 3). Importantly, this observed symmetry mismatch is apparent in the 3D reconstructions of both native MCU_{NC} and BS3-crosslinked MCU_{NC} (fig. S3). Local and global alignments of protomers A and B in the MCU_{NC} structure indicate the domain rearrangements between the TMD and the CCD-NTD account for the symmetry break (Fig. 3 and fig. S9) with the departure from 4-fold symmetry originating from two distinct interaction networks engaged by neighboring NTDs (Fig. 3). With respect to the NTDs and CCDs, the channel adopts a dimer-of-dimers assembly; within the NTD dimer comprising

protomers A and B (the A/B dimer), there is a large dimer interface (~620 $Å^2$) defined by both NTDs and CCDs, while there is a comparatively minimal dimer interface (~380 $Å^2$) mediated by the NTD dimer comprising protomers B and C (the B/C dimer).

The dimer-of-dimers assembly of soluble domains and the tetrameric assembly of the TMD in MCU_{NC} is analogous to that of ionotropic glutamate receptors (iGluRs) (27). In iGluRs, the ligand binding domain (LBD) and amino terminal domain (ATD) assume 2-fold symmetric arrangements, while the TMD adopts a 4-fold symmetric arrangement. The LBD transitions into various conformations, including a pseudo-four-fold arrangement during the gating cycle of iGluR (28, 29), indicating the NTD dimer-of-dimers assembly might play a comparable role in MCU gating. This notion is further supported by recent studies suggesting that phosphorylation of the NTD or divalent cation binding to the NTD modulate MCU function (fig. S7) (20, 21).

Many structural and architectural features observed in our MCU_{NC} structure contrast with those of cMCU-ΔNTD (Fig. 4). First, cMCU-ΔNTD and MCU_{NC} adopt distinct pentameric and tetrameric stoichiometries, respectively, which could result from construct design (truncation of the NTD versus full-length protein), choice of detergents (zwitterionic Fos-choline-14 versus dodecylmaltoside), and/or protein preparation (extraction from inclusion body versus the membrane). The Ca^{2+} channel function has not been shown in either cMCU (22) nor MCU_{NC}. Therefore, the *in vivo* oligomeric status of MCU has not been established and we cannot exclude the possibility that fungal and cMCUs may adopt different oligomeric arrangements. These discrepancies await further validation. Second, the arrangement of TM1 and TM2 in MCU_{NC} establishes an extensive inter-protomer interface, whereas the TM helices in cMCU-ΔNTD only form intra-protomer interactions. Third, while the selectivity filter sequence is located on TM2 in MCU_{NC}, the corresponding residues in cMCU-ΔNTD are positioned within a loop, leading to different selectivity filter structures (fig. S10). Finally, the CCD in MCU_{NC} consists of four dimeric coiled coils, formed by CC1 and CC2, whereas the CC2 from each protomer in cMCU-ΔNTD forms a pentameric coiled coil in the CCD (Fig. 4).

Our studies provide structural insights into the design principle of the MCU_{NC} selectivity filter, which will serve as a platform to understand the mechanism of selective calcium permeation by this channel family.

Supplementary Material

Refer to Web version on PubMed Central for supplementary material.

Acknowledgments:

Cryo-EM data were collected at The Scripps Research Institute (TSRI) electron microscopy facility. We thank Alvin Kuk and Yang Suo at Duke University who helped with calcium flux experiments and preliminary negative-staining EM analyses, respectively. We thank Jean-Christophe Ducom at TSRI High Performance Computing facility for computational support and Bill Anderson for microscope support. We thank S. Y. Kim at Duke Functional Genomics Shared Resource for generating the human MCU knock-out cell line.

Funding: This work was supported by the National Institutes of Health (R35NS097241 to S.-Y. L., DP2EB020402 and R21AR072910 to G.C.L.). G.C.L is supported as a Searle Scholar and a Pew Scholar. Computational analyses of EM data were performed using shared instrumentation funded by NIH S10OD021634.

Reference and Notes:

1. Mammucari C, Gherardi G, Rizzuto R, Structure, Activity Regulation, and Role of the Mitochondrial Calcium Uniporter in Health and Disease. Front Oncol 7, 139 (2017). [PubMed: 28740830]
2. Kamer KJ, Mootha VK, The molecular era of the mitochondrial calcium uniporter. Nat Rev Mol Cell Biol 16, 545–553 (2015). [PubMed: 26285678]
3. Gunter TE, Pfeiffer DR, Mechanisms by which mitochondria transport calcium. Am J Physiol 258, C755–786 (1990). [PubMed: 2185657]
4. Kirichok Y, Krapivinsky G, Clapham DE, The mitochondrial calcium uniporter is a highly selective ion channel. Nature 427, 360–364 (2004). [PubMed: 14737170]
5. Baughman JM et al., Integrative genomics identifies MCU as an essential component of the mitochondrial calcium uniporter. Nature 476, 341–345 (2011). [PubMed: 21685886]
6. Perocchi F et al., MICU1 encodes a mitochondrial EF hand protein required for Ca(2+) uptake. Nature 467, 291–296 (2010). [PubMed: 20693986]
7. De Stefani D, Raffaello A, Teardo E, Szabo I, Rizzuto R, A forty-kilodalton protein of the inner membrane is the mitochondrial calcium uniporter. Nature 476, 336–340 (2011). [PubMed: 21685888]
8. Sancak Y et al., EMRE is an essential component of the mitochondrial calcium uniporter complex. Science 342, 1379–1382 (2013). [PubMed: 24231807]
9. Raffaello A et al., The mitochondrial calcium uniporter is a multimer that can include a dominant-negative pore-forming subunit. EMBO J 32, 2362–2376 (2013). [PubMed: 23900286]
10. Kamer KJ, Mootha VK, MICU1 and MICU2 play nonredundant roles in the regulation of the mitochondrial calcium uniporter. EMBO Rep 15, 299–307 (2014). [PubMed: 24503055]
11. Tsai MF et al., Dual functions of a small regulatory subunit in the mitochondrial calcium uniporter complex. Elife 5, (2016).
12. Hoffman NE et al., MICU1 motifs define mitochondrial calcium uniporter binding and activity. Cell Rep 5, 1576–1588 (2013). [PubMed: 24332854]
13. Kamer KJ, Grabarek Z, Mootha VK, High-affinity cooperative Ca(2+) binding by MICU1-MICU2 serves as an on-off switch for the uniporter. EMBO Rep 18, 1397–1411 (2017). [PubMed: 28615291]
14. Csordas G et al., MICU1 controls both the threshold and cooperative activation of the mitochondrial Ca(2)(+) uniporter. Cell Metab 17, 976–987 (2013). [PubMed: 23747253]
15. Mallilankaraman K et al., MICU1 is an essential gatekeeper for MCU-mediated mitochondrial Ca(2+) uptake that regulates cell survival. Cell 151, 630–644 (2012). [PubMed: 23101630]
16. Bick AG, Calvo SE, Mootha VK, Evolutionary diversity of the mitochondrial calcium uniporter. Science 336, 886 (2012). [PubMed: 22605770]
17. Kovacs-Bogdan E et al., Reconstitution of the mitochondrial calcium uniporter in yeast. Proc Natl Acad Sci U S A 111, 8985–8990 (2014). [PubMed: 24889638]
18. Song J, Liu X, Zhai P, Huang J, Lu L, A putative mitochondrial calcium uniporter in A. fumigatus contributes to mitochondrial Ca(2+) homeostasis and stress responses. Fungal Genet Biol 94, 15–22 (2016). [PubMed: 27378202]
19. Wu G et al., Single channel recording of a mitochondrial calcium uniporter. Biochem Biophys Res Commun 496, 127–132 (2018). [PubMed: 29307826]
20. Lee Y et al., Structure and function of the N-terminal domain of the human mitochondrial calcium uniporter. EMBO Rep 16, 1318–1333 (2015). [PubMed: 26341627]
21. Lee SK et al., Structural Insights into Mitochondrial Calcium Uniporter Regulation by Divalent Cations. Cell Chem Biol 23, 1157–1169 (2016). [PubMed: 27569754]
22. Oxenoid K et al., Architecture of the mitochondrial calcium uniporter. Nature 533, 269–273 (2016). [PubMed: 27135929]

23. Hou X, Pedi L, Diver MM, Long SB, Crystal structure of the calcium release-activated calcium channel Orai. Science 338, 1308–1313 (2012). [PubMed: 23180775]
24. Saotome K, Singh AK, Yelshanskaya MV, Sobolevsky AI, Crystal structure of the epithelial calcium channel TRPV6. Nature 534, 506–511 (2016). [PubMed: 27296226]
25. Doyle DA et al., The structure of the potassium channel: molecular basis of K+ conduction and selectivity. Science 280, 69–77 (1998). [PubMed: 9525859]
26. Hirschi M et al., Cryo-electron microscopy structure of the lysosomal calcium-permeable channel TRPML3. Nature 550, 411–414 (2017). [PubMed: 29019979]
27. Sobolevsky AI, Rosconi MP, Gouaux E, X-ray structure, symmetry and mechanism of an AMPA-subtype glutamate receptor. Nature 462, 745–756 (2009). [PubMed: 19946266]
28. Twomey EC, Yelshanskaya MV, Grassucci RA, Frank J, Sobolevsky AI, Channel opening and gating mechanism in AMPA-subtype glutamate receptors. Nature 549, 60–65 (2017). [PubMed: 28737760]
29. Twomey EC, Sobolevsky AI, Structural Mechanisms of Gating in Ionotropic Glutamate Receptors. Biochemistry 57, 267–276 (2018). [PubMed: 29037031]
30. Smart OS, Neduvelil JG, Wang X, Wallace BA, Sansom MS, HOLE: a program for the analysis of the pore dimensions of ion channel structural models. J Mol Graph 14, 354–360, 376 (1996). [PubMed: 9195488]

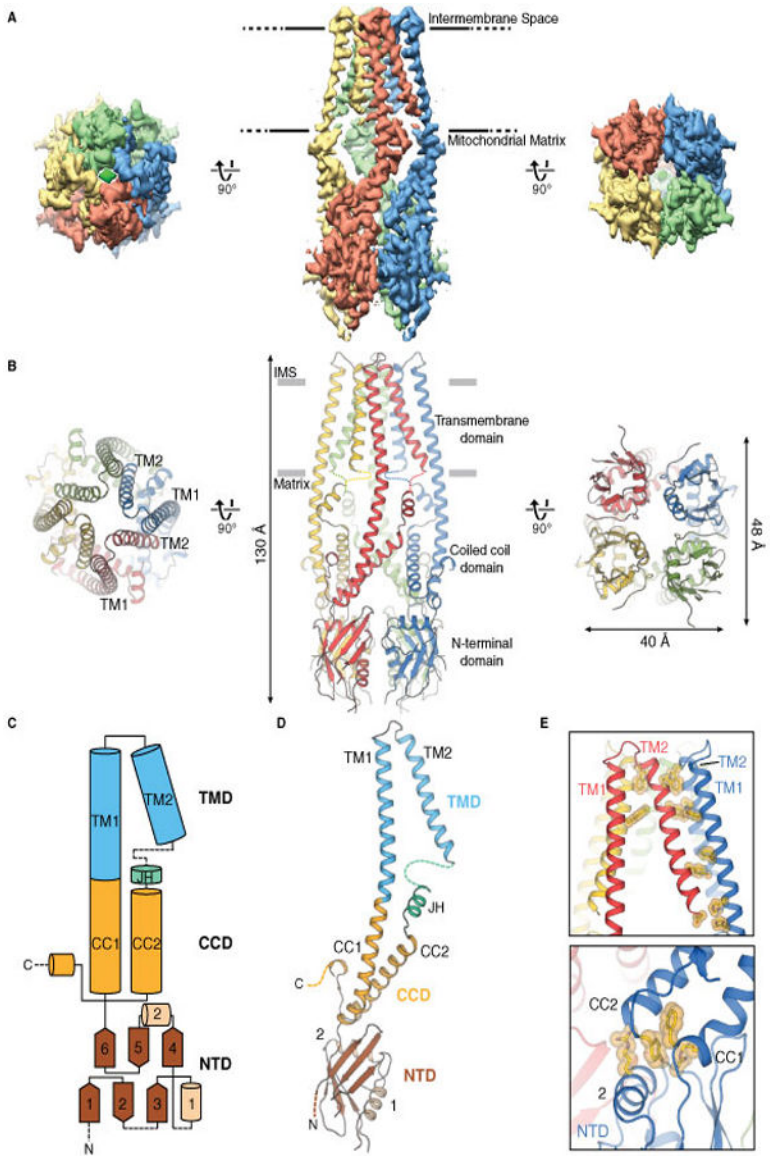

Figure 1. Overall architecture of MCU_{NC}.

(**A**) Single-particle cryo-EM reconstruction and (**B**) model of MCU_{NC} viewed from the intermembrane space (left), within the inner mitochondrial membrane (middle), and from the mitochondrial matrix (right). (**C**) Cartoon diagram outlining the protein domains and secondary structures. (**D**) Detailed view of an MCU protomer as colored in (C). Dashed lines indicate parts that were not modeled in the structure. (**E**) Close-up views of interactions between TM2 and TM1 from neighboring protomers (upper), between CCD and α2 from NTD (lower).

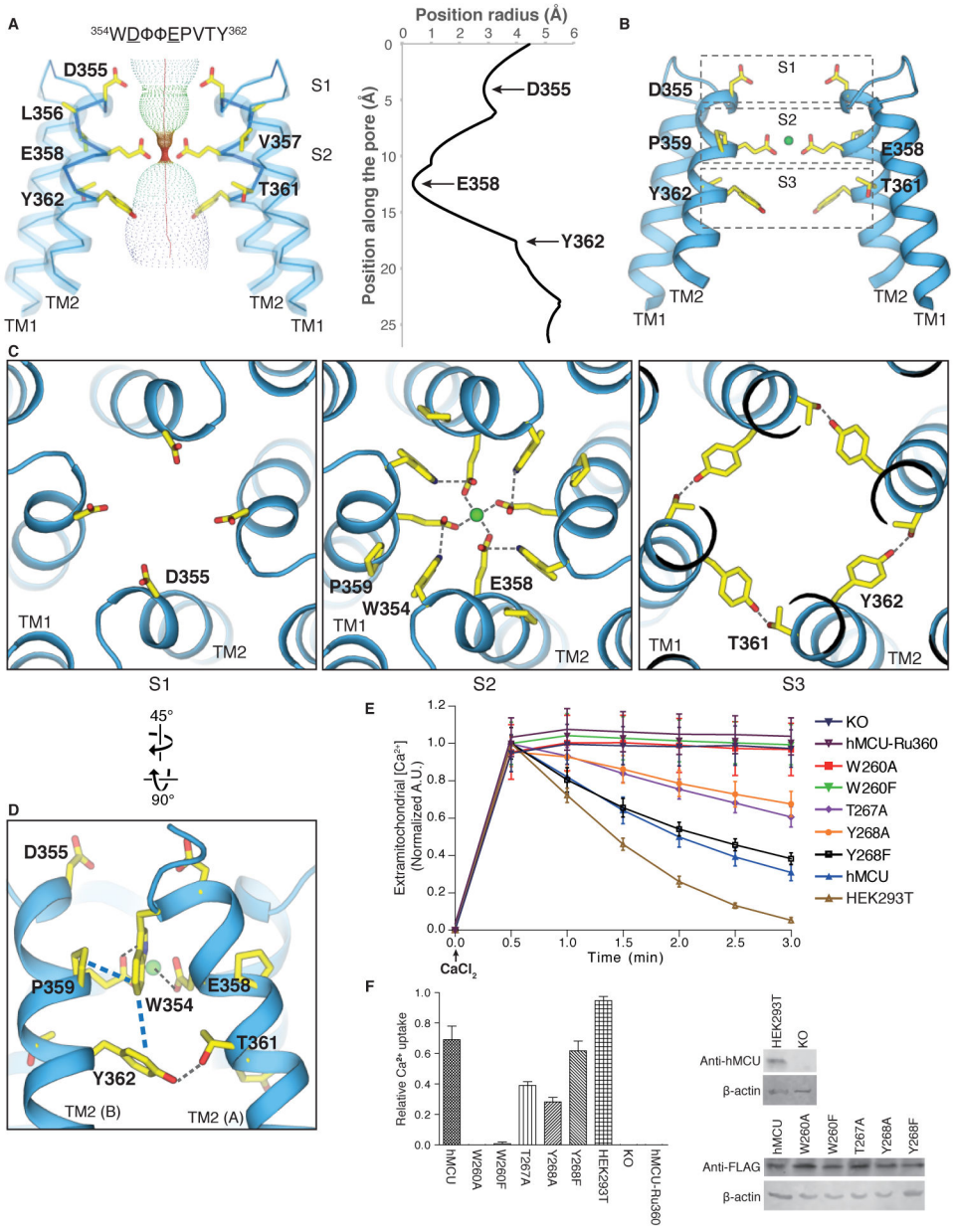

Figure 2. Ion conduction pore and selectivity filter.

(**A**) The ion conduction pathway of MCU_{NC} and the pore radius along the central axis (generated with HOLE software (30)) indicate three constrictions at Asp^{355}, Glu^{358}, and Tyr^{362}. Front and rear protomers were removed for clarity. (**B**) Putative Ca^{2+} coordination sites, among which a strong cryoEM density peak was observed and tentatively modeled as Ca^{2+} at site 2. (**C**) Top views of the putative Ca^{2+} coordination sites constituted by Asp^{355} at S1 (left), by Trp^{354}, Glu^{358}, and Pro^{359} at S2 (middle), and by Thr^{361} and Tyr^{362} at S3 (right). **(D)** Detailed view from the membrane plane showing the extensive network of interactions engaged by residues in the "WDΦΦEPVTY" motif. The CH-**π** (Pro^{359} and Trp^{354}) and **π-π** (Trp^{354} and Tyr^{362}) interactions are highlighted by blue dashed lines. (**E**) Mitochondrial calcium uptake of human MCU (hMCU) mutants from MCN_{NC} structure-

based mutagenesis at the ion conduction pore. Representative traces of calcium uptake in digitonin-permeabilized cells after 10 μM $CaCl_2$ was added. Mutation of Trp^{260} to Ala or Phe suppresses hMCU channel function, whereas mutation of Thr^{267} or Tyr^{268} to Ala solely reduces the activity. Mutation of Tyr^{268} to Phe shows calcium uptake to the comparable extent as wildtype hMCU (hMCU) expressed in MCU knockout (KO) cells. (**F**) Bar graph showing the calcium uptake of hMCU mutants relative to the wildtype hMCU between 0.5 and 3-min time points (mean ± SEM, n ≥ 4 independent measurements). To detect the expression of hMCU mutants, cell lysates were analyzed by immunoblotting with anti-FLAG antibody. Wild-type HEK 293T cells and MCU knockout cells were confirmed by anti-hMCU antibody. β-actin was used as the loading control.

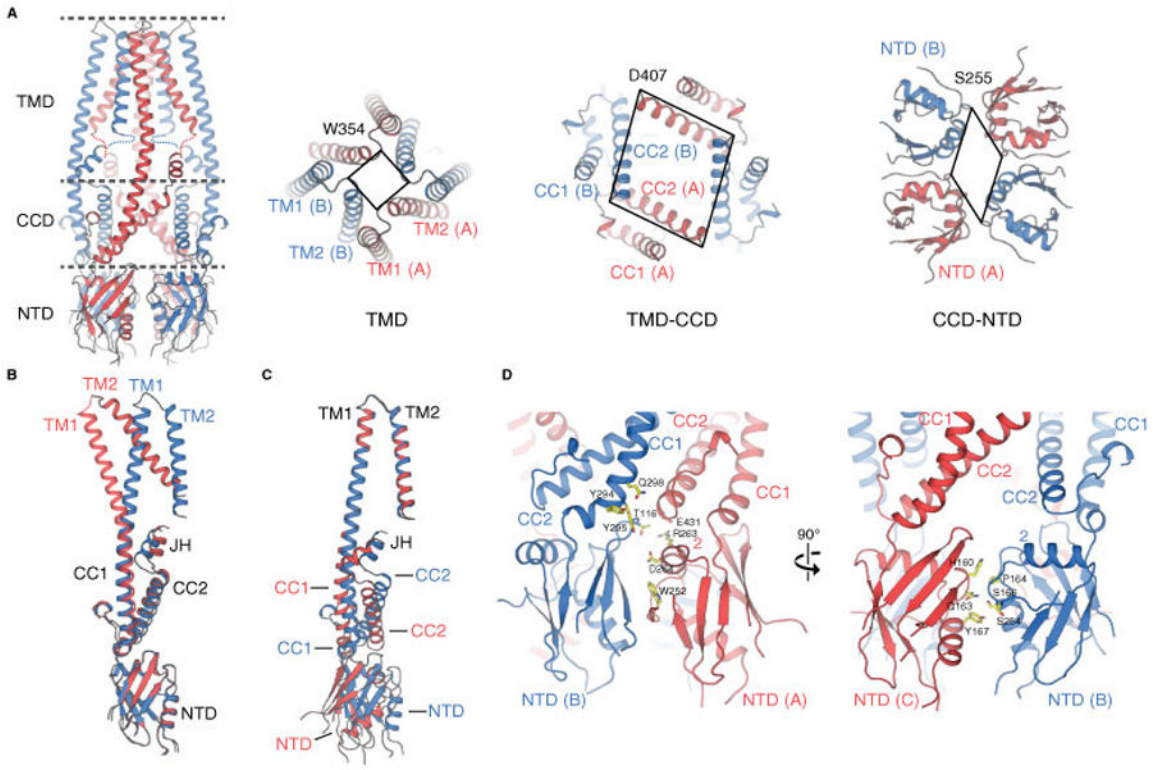

Figure 3. Hinge rotation enables the mismatch in channel symmetry.

(**A**) Top view comparison of channel symmetry sliced through the three layers depicted in the tetrameric MCU_{NC} channel. The TMD exhibits 4-fold symmetry, while both the CCD and NTD display 2-fold symmetry. The lines are drawn between Cα atoms of Trp^{354}, Asp^{407}, and Ser^{255}. (**B and C**) Alignment of protomer A (red) and protomer B (blue) at NTD (**B**) and at TMD (**C**), showing the rigid body rotations of TMD and NTD around the hinge point JH. (**D**) Distinct interfacial networks between each NTD and its neighboring partner.

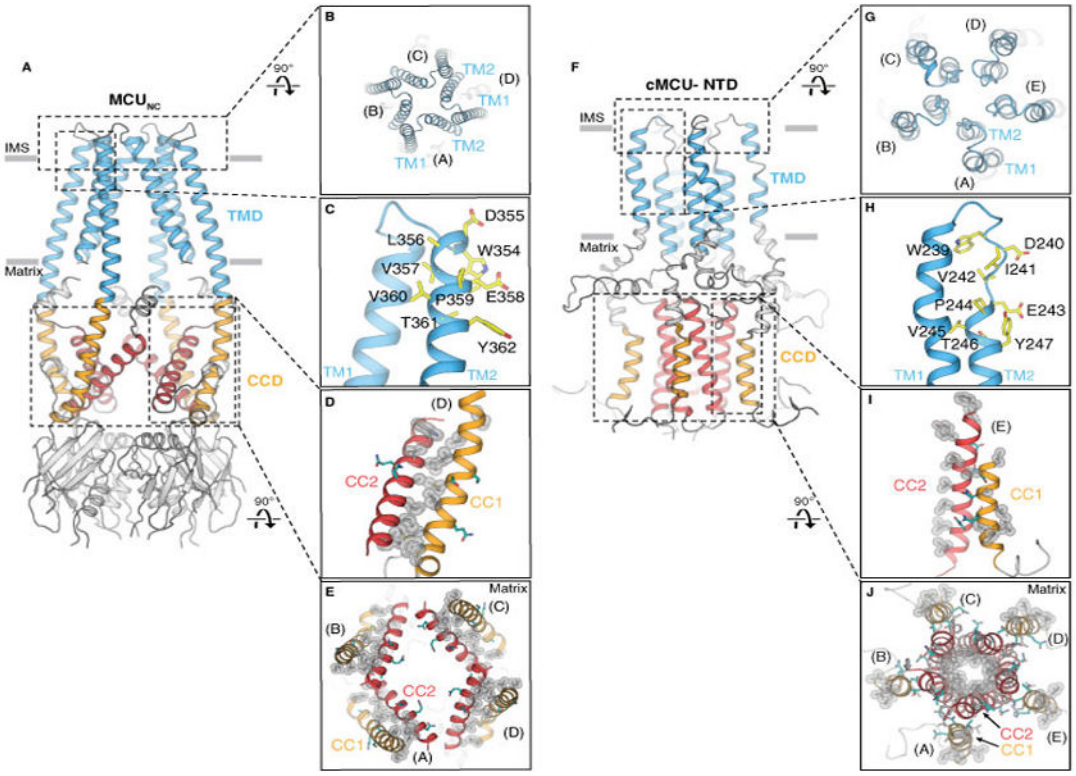

Figure 4. Comparison of cryo-EM structure MCU$_{NC}$ and NMR structure cMCU-ΔNTD.

(**A and B**) Side and top views showing the tetrameric configuration of MCU$_{NC}$. (**C**) The selectivity filter sequence (yellow) of MCU$_{NC}$ is located at the beginning of TM2. (**D**) Close-up view of the hydrophobic interactions (silver spheres) between CC1 and CC2. Hydrophilic residues are colored in teal. (**E**) Viewed from the intermembrane space, CC1 (orange) and CC2 (red) of MCU$_{NC}$ form dimeric coiled coils within each protomer via extensive hydrophobic interactions (highlighted by silver spheres). (**F and G**) Side and top views showing cMCU-ΔNTD (PDB ID: 5ID3) forms a pentamer. (**H**) The "DΦΦE" motif (yellow) in cMCU is located at the loop connecting TM1 and TM2. (**I**) Close-up view of the hydrophobic residues (silver spheres) located on CC1 and CC2. Hydrophilic residues are colored in teal. (**J**) Viewed from the intermembrane space, CC2 (red) forms a pentameric helical bundle via hydrophobic interactions (silver spheres) pointing towards the central axis. Hydrophobic residues (silver spheres) on CC1 (orange) are exposed to the mitochondrial matrix.